Improved fuzzy logic method to distinguish between meteorological and non-meteorological echoes using C-band polarimetric radar data

Shuai Zhang[1,2], Xingyou Huang[1], Jinzhong Min[2], Hengheng Zhang[1]

5 [1]School of Atmospheric Physics, Nanjing University of Information Science and Technology, Nanjing, China
[2]School of Atmospheric Sciences, Nanjing University of Information Science and Technology, Nanjing, China

Correspondence to: Xingyou Huang (huangxy@nuist.edu.cn)

Abstract. In order to obtain better performance of meteorological applications, it is necessary to distinguish radar echoes from meteorological and non-meteorological targets. After the comprehensive analysis of the computational efficiency and

10 radar system characteristics, a fuzzy logic method similar to the MetSignal algorithm is adopted, but its performance is improved significantly in weak signal regions where polarimetric variables are severely affected by noise. In addition, post-processing is adjusted to prevent anomalous propagation at far range to be misclassified as meteorological echo. Moreover, an additional fuzzy logic echo classifier is introduced into post-processing to suppress misclassification in the melting layer. An independent test set is selected to evaluate algorithm performance, and the statistical results show that the performance of

15 the algorithm has been significantly improved, especially with respect to the classification of meteorological echoes in weak signal regions.

1 Introduction

Weather radar with dual-polarization capability has a wider range of application than conventional weather radar (i.e., single-polarization weather radar), in terms of providing information regarding the shape, size, spatial orientation, and physical

20 composition of hydrometeors (Kumjian 2013a; Kumjian 2013b; Kumjian 2013c). Significant improvements have been made in meteorological and hydrological applications (e.g., data assimilation, quantitative precipitation estimation, and hydrometeor classification) on using polarimetric radar data (Giangrande and Ryzhkov 2008; Jung et al. 2008a; Jung et al. 2008b; Park et al. 2009). However, the existence of non-meteorological echoes (NMET; e.g., ground clutter (GC), anomalous propagation (AP), and clear-air echoes (CA)) in radar data often discounts the application performance. Therefore,

25 it is necessary to separate radar data that contain meteorological echoes (MET; e.g., rain, snow, and hail) from those that contain NMET before these applications are implemented.

Several effective algorithms for distinguishing between NMET and MET have been proposed in recent years. Lakshmanan et al. (2014) developed an algorithm based on neural networks for radar data quality control. The raw values and local variance of polarimetric variables and Doppler moments, as well as features calculated from 3D virtual volume, are selected

30   as the input of the neural network. The output of the neural network is the probability of MET at each range gate. The range
gates are then clustered into contiguous regions and the probabilities are averaged within each cluster. The average
probability is compared with a preset probability threshold to determine whether the cluster is retained (considered as MET)
or censored (considered as NMET). A MET–NMET classifier was developed by Tang et al. (2014) to perform reflectivity
data quality control using polarimetric radar variables and atmospheric environmental data. The algorithm combines a simple
35   correlation coefficient filter as the primary determinant and applies a set of physically-based rules to handle some special
MET (e.g., hail, non-uniform beam filling, and melting layer (ML)) and NMET (e.g., random clutter with high correlation
coefficient). Krause (2016) proposed an algorithm, MetSignal, to distinguish between MET and NMET using polarimetric
radar data, which has a simple design and allows users to adjust its performance according to the specific situation. The
MetSignal algorithm is based on fuzzy logic technique with a few post-processing rules; it has been selected to be
40   implemented on the WSR-88D network in the United States. In addition, the performance of different methods in the context
of distinguishing between MET and NMET is compared in Rico-Ramirez and Cluckie (2008) and Islam et al. (2012). Further,
the importance of different features is also evaluated by Lakshmanan et al. (2015).

Compared with the other two methods (Tang et al. 2014; Krause 2016), the most obvious disadvantage of the neural network
method proposed by Lakshmanan et al. (2014) is the heavy computation intensity, which is not suitable in operation
45   application, especially for radar systems with high spatial and/or temporal resolution. Although the method proposed by
Tang et al. (2014) has a higher computational efficiency than the method proposed by Lakshmanan et al. (2014), it may
result in undesirable performance if applied in polarimetric radar systems with imperfect hardware technology or without
noise correction (Gourley et al. 2006; Schuur et al. 2003), which is mainly attributed to excessive dependence on the
correlation coefficient. Fuzzy logic is a multiple-input classifier method, which can minimize the impact from a single
50   erroneous input. In addition, the MetSignal algorithm has the highest computational efficiency among the three methods
(Krause 2016; Tang et al. 2014). Therefore, a similar framework adopted in the MetSignal algorithm is used in this paper.

The MetSignal algorithm, like most methods distinguishing between MET and NMET based on polarimetric radar data, has
high expectations for polarimetric features and sets a high weight for these. However, the fluctuation of polarimetric
variables in the weak signal regions and the regions affected by ML is very intense, which shows characteristics similar to
55   NMET and is not conducive to distinguishing between MET and NMET (Krause 2016; Rico-Ramirez and Cluckie 2008).
The suppression of misclassification in ML regions is added in the post-processing of the MetSignal algorithm, but lack of
consideration for weak signal regions where polarimetric variables severely affected by noise. The main purpose of the
method proposed in this paper is to improve the performance of the MetSignal algorithm in weak signal regions, hence it is
called MetSignal_noise. In addition, some other adjustments and improvements over the MetSignal algorithm are also
60   included in the MetSignal_noise algorithm.

The rest of this paper is organized as follows. Section 2 briefly describes the radar system and data used in this study and the
available measurements. A detailed explanation of the proposed algorithm is provided in Section 3 and Section 4 presents
the evaluation result of the algorithm performance. Finally, conclusions are provided in Section 5.

2 Instrument and data

65 The radar data used in this study were collected by a C-band dual-polarization Doppler weather radar owned by the Nanjing University of Information Science and Technology (NUIST-CDP). The main parameters of NUIST-CDP are listed in Table 1. NUIST-CDP is designed and manufactured by Beijing Metstar Radar Company in China and deployed on the university campus (32.21 °N, 118.72 °E). The routine scanning mode of NUIST-CDP is volume scanning with 14 elevation angles (0.5, 1.5, 2.4, 3.4, 4.3, 5.3, 6.2, 7.5, 8.7, 10, 12, 14, 16.7, and 19.5°) and updated scanned every 7-min. The available

70 measurements include the reflectivity factor at horizontal polarization (Z), Doppler velocity (V), Doppler spectrum width (W), differential reflectivity (ZDR), differential propagation phase shift (PhiDP), co-polar correlation coefficient (CC), signal-to-noise ratio (SNR), and signal quality index, all at a radial range resolution of 75 m.

The NUIST-CDP radar data are seriously affected by GC and AP, which is attributed to the absence of clutter filtering in the signal processing. The strong CA is one of main sources of error for some meteorological and hydrological applications

75 (Stumpf et al. 1998; Zhang et al. 2011), which often appears in NUIST-CDP radar data during the warm season. In addition, NUIST-CDP has a higher pulse repetition frequency than the operational radar (Crum et al. 1993), which means a shorter maximum detection range and more frequent second-trip echoes. Considering that the second-trip echo is formed by meteorological targets, the algorithm temporarily classifies it as MET. The identification and removal of second-trip echoes will be considered in future research.

80 3 Method

3.1 MetSignal

Since a similar algorithm framework is used in both MetSignal and MetSignal_noise, a brief description of the MetSignal algorithm is presented first. As shown in Fig. 1, the major steps of the MetSignal algorithm is summarized as a block diagram.

85 Except for the raw radar variables (i.e., Z, V, and CC), two texture parameters (i.e., SD(ZDR) and SD(CC)) also input into the fuzzy logic echo classifier as features. The SD(ZDR) and SD(CC) are estimated by calculating standard deviations of ZDR and CC along a radial for 21 range gates (1.5 km in NUIST-CDP) centered on the target gate, which can characterize the magnitude of small-scale fluctuations in ZDR and CC. It is worth noting that the SD(PhiDP) input in the raw version of MetSignal was removed to avoid texture estimation errors because of phase folding. Although there are some conventional

90 methods to solve phase folding (Wang and Chandrasekar 2009), they fail when applied to radar data mixed with first- and second-trip echoes.

The fuzzy logic technique is applied in the echo classifier, which is a classification methodology widely used in the weather radar community (Gourley et al. 2007; Lin et al. 2012; Liu and Chandrasekar 2000). The fuzzy logic of the additive version is applied to obtain the aggregation value for the MET (A_{MET}) to maximize the probability of detection (Zrnić et al. 2001):

95    $A_{MET} = \frac{\sum W_x MF_x}{\sum W_x}$, (1)

where x is one of the five features mentioned above, and W_x and MF_x are the weight (the weight setting for each feature is shown in Table 2) and membership function value of x, respectively. The A_{MET} is then compared to a preset threshold (0.8 in the warm season and 0.7 in the cold season). The target gate will be classified as MET if A_{MET} exceeds the preset threshold; otherwise, it will be classified as NMET.

100   For the classification method using fuzzy logic, the selection of membership functions often determines the final classification performance to a certain extent. In addition, considering that the characteristics of radar variables depend on the radar systems as well as the climatological and geographical location of the radar, the membership functions are objectively determined by the statistical analysis of measured data from NUIST-CDP. The data used for training are summarized in Table 3, which consist of several typical events including GC, AP, CA, stratiform precipitation, and

105   convective precipitation.

The normalized frequency distributions of features are shown in Fig. 2, which are derived using the training set listed in Table 3. The method proposed by Cho et al. (2006) is used to determine the membership functions; it has a higher efficiency than the iterative method used in Krause (2016):

$MF_x = \frac{FMET_x}{FMET_x + FNMET_x}$, (2)

110   where FMET and FNMET are the normalized frequencies of MET and NMET. The trapezoidal functions are adopted to indicate the membership functions by fitting the results of Eq. (2) using the least-squares method (the red lines in Fig. 2).

After obtaining the preliminary results of the fuzzy logic echo classifier, a set of post-processing rules are applied to adjust the classification results appropriately to make them more reasonable. These rules include a ZDR filter for eliminating residual CA (the range gates with absolute value of ZDR exceeding 4.5 dB are considered as NMET), a CC filter (the range

115   gates with CC less than 0.65 are considered as NMET), and forced classification as MET will also be performed in range gates where Z at a height of 3 km in the previous volume scan at the same location exceeds 11 dBZ, which will help to prevent misclassification of the algorithm in ML regions.

3.2 Improvements and adjustments in MetSignal_noise

3.2.1 The limitation of the use scope of V

120   As shown in Fig. 2b, although the V of NMET is mainly concentrated near 0 m/s while the V of MET is uniformly distributed in the whole range, there is still a large overlap between them in the regions where the absolute value of V is large. The broadening of the frequency distribution of NMET is mainly attributed to the existence of CA, which is similar to that of MET in terms of V (Wilson et al. 1994). Considering that the V does not play a role in distinguishing MET from CA, some constraint conditions should be set to limit the use scope of V in fuzzy logic echo classifier. Since the CA usually has

125   smaller Z and larger W than GC and AP (Fang et al. 2004; Wilson et al. 1994), a 2D histogram method is adopted to analyse the relationships of V vs Z and V vs W of NMET in the training set listed in Table 3 to find the thresholds of Z and W for separating CA from other NMET, as far as possible. As shown in Fig. 3a, the 2D histogram of V vs Z of NMET presents an orthogonal shape, which is composed of GC and AP with V near 0 m/s and CA with Z below 30 dBZ and V uniformly distributed in the whole range. As shown in Fig. 3b, the 2D histogram of V vs W of NMET is uniform on the whole, except

130   for the region where V is close to 0 m/s and W is less than 2 m/s. This region is very concentrated and should be composed of GC and AP due to its static and stable characteristics. Therefore, the V is used in fuzzy logic echo classifier as a feature only when Z is greater than 30 dBZ or W is less than 2 m/s. The normalized frequency distribution and membership function of V after setting thresholds of Z and W is shown in Fig. 3c. Compared with Fig. 2b, the frequency distribution of NMET in Fig. 3c is more concentrated at 0 m/s, and the broadening has also been significantly reduced, while that of MET remains

135   uniformly distributed in the whole range without notable changes.

3.2.2 The decrease of CC in the region of GC and AP

As shown in Fig. 2c, there is a significant overlap between NMET and MET in the region where CC is above 0.8, which increases difficulty in distinguishing between NMET and MET and is contrary to the common knowledge that NMET has a low CC (Kumjian 2013a). After analysing a large amount of data, it is found that NMET of high CC mainly comes from the

140   GC and AP, which may be due to the characteristics of the NUIST-CDP radar (e.g., spatial resolution and dwelling time). Therefore, the method proposed by Zrnić et al. (2006)—CC is averaged along the radial using a 21-range gates window (1.5 km in NUIST-CDP)—is adopted to reduce the CC of NMET with the abnormal high value. As shown in Fig. 4, it is a typical case of AP (23:53 UTC 24 May 2017) sampled by the NUIST-CDP radar. Compared with the raw CC in Fig. 4b, where some regions of GC and AP have high CC, the CC after average processing in Fig. 4c decreased significantly in these

145   regions and almost all of them are below 0.9, which is expected to improve classification performance to some extent.

3.2.3 The improvements in weak signal region

As shown in Fig. 5, the NUIST-CDP radar observed a typical case of mixed precipitation accompanied by CA within 50 km (13:24 UTC 30 May 2017). A comprehensive analysis of A_{MET} obtained by the MetSignal algorithm (Fig. 5a) as well as Z (Fig. 5b) and SNR (Fig. 5c) reveals that MET with lower SNR near the echo edge have lower A_{MET} than MET in the core

150   regions with larger SNR, which even close to the A_{MET} of CA. This is because the estimation accuracy of polarimetric variables usually depends on SNR (Bringi and Chandrasekar 2001). As shown in Figs. 5d and 5e, significant fluctuation of ZDR and decrease of CC can be found near the echo edge. Meanwhile, their derivatives (i.e., SD(ZDR) in Fig. 5f and SD(CC) in Fig. 5g) have also increased significantly in these regions.

In order to understand the dependence between polarimetric features and SNR in more detail, a boxplot method is adopted to

155   analyse the MET in the training set listed in Table 3. As shown in Fig. 6a, the boxplot of SNR vs ZDR takes the shape of a dumbbell. The broadening distribution of ZDR with the increase of SNR is attributed to the large raindrops, strong

attenuation, and the resonance effect produced by hailstones, which is easy to be understood and corresponds to common knowledge (Kumjian 2013c). The MET with smaller SNR usually consists of drizzle, dry snow, and even cloud particles, which should have ZDR close to 0 dB and hence, is often used in ZDR calibration as natural targets (Ryzhkov et al. 2005).

160 Therefore, the ZDR broadening with the decrease of SNR should not be attributed to microphysical properties of MET but the artifacts owing to the influence of noise. Similarly, as shown in Fig. 6b, the magnitude (dispersion) of CC decreases (increases) with decrease of SNR when SNR is less than 15 dB. These anomalies in ZDR and CC should be attributed to the weak signal affected by noise, which leads to the polarimetric variables being unable to represent the real microphysical information in MET, and also leads to high value of SD(ZDR) (Fig. 6c) and SD(CC) (Fig. 6d).

165 Considering the dependence between polarimetric features and SNR, the polarimetric features are stratified by three SNR intervals (less than 5 dB, 5–15 dB, and larger than 15 dB) and different processing methods are used for each of these intervals. First, the data of SNR less than 5 dB are directly regarded as noise and not classified. This is because the MET in this interval is seriously affected by noise and also too weak to play an important role in meteorological and hydrological applications. In addition, as polarimetric variables with low SNR may increase the texture of adjacent gates, the method

170 proposed by Rico-Ramirez and Cluckie (2008)—masking the polarimetric variables of SNR less than 5 dB in texture calculation—is adopted to reduce the risk of misclassification. Then, the normalized frequency distributions of polarimetric features in Fig. 2 are separated based on different SNR intervals (i.e., 5–15 dB and larger than 15 dB) and the results are shown in Fig. 7. As shown in Figs. 7a and b, the long trailing of CC of the MET caused by low SNR in Fig. 2c is well distinguished from the "normal" MET that has CC close to 1 and no less than 0.8. In addition, the odd bimodal distributions

175 of SD(ZDR) (Fig. 2d) and SD(CC) (Fig. 2e) are also well decomposed after stratification by SNR (Figs. 7c, d, e, and f), which makes the membership functions more pertinent and can better characterize the polarimetric features in different SNR intervals.

The A_{MET} obtained by the MetSignal_noise algorithm is shown as Fig. 8a. In order to better compare the performance of the MetSignal and MetSignal_noise algorithms, the A_{MET} obtained by the MetSignal algorithm with SNR less than 5 dB is

180 masked (Fig. 8b). The difference between them is mainly reflected in the regions of echo edge and near the radar, which is mainly contributed by two factors. First, the fluctuation of polarimetric variables is reduced by masking the polarimetric variables of low SNR (Figs. 8c and 8d), and the texture of polarimetric variables affected by noise is significantly alleviated (Figs. 8e and 8f). Second, the polarimetric features can characterize MET and NMET more detailed by adjusting the membership functions based on different SNR intervals (Fig. 7).

185 3.2.4 Adjustments of post-processing for ML region

The last step in the post-processing of MetSignal algorithm is to check the constant-altitude plan position indicator (CAPPI) of Z at 3 km in the previous volume scan. The range gates will be force-classified as MET if the CAPPI at the same location exceeds 11 dBZ; this aims to prevent the misclassification in ML regions. However, due to the strong super-refraction caused by specific weather conditions (Doviak and Zrnić 2006), NUIST-CDP radar sometimes detects AP more than 11 dBZ

190   at a far range (corresponding to an altitude higher than 3 km), which will misclassify AP as MET after post-processing. Fig. 9 shows the same AP case as in Fig. 4. Although the A_{MET} obtained by the MetSignal algorithm has a low value (Fig. 9a), which means that the classification result tends to NMET; there are still many range gates misclassified as MET in the final result (Fig. 9b) due to improper post-processing. As there is a potential risk of misclassification of AP into MET in this post-processing step, it is removed in MetSignal_noise.

195   However, the lack of special precaution in the ML regions makes misclassification a frequent occurrence, which is due to the fact that MET in ML regions and NMET have similar characteristics in polarimetric features. Therefore, an additional fuzzy logic echo classifier without the polarimetric features input is implemented in post-processing of MetSignal_noise in the potential ML regions (initially defined as the regions over 2.5 km in height) for range gates classified as NMET in the first fuzzy logic echo classifier. Considering that AP in the potential ML regions may not be classified effectively by solely using

200   Z and V, the SD(Z) (using the same estimation method as SD(ZDR) and SD(CC)) is added to improve the classification performance. The normalized frequency distribution and membership function of SD(Z) are shown in Fig. 10, which are also derived from the training set listed in Table 3 but only using data in the potential ML regions. If these range gates (classified as NMET in the first fuzzy logic echo classifier in the potential ML regions) are classified as MET in the additional fuzzy logic echo classifier, then they are likely to be influenced by ML and should be reclassified as MET.

205   As shown in Fig. 11, the NUIST-CDP radar observed a typical case of stratiform precipitation (10:49 UTC 23 May 2017). Although the bright band characteristic of Z is not very obvious (Fig. 11d), the location of ML region at a range of about 100 km can be well revealed by ZDR and CC (Figs. 11e and 11f). As shown in Fig. 11b, the A_{MET} before post-processing (the result of the first fuzzy logic echo classifier) has a significant decrease in the ML region, which is due to the similar characteristics of polarimetric features between MET in ML regions and NMET. The A_{MET} after post-processing (the range

210   gates classified as NMET in the first fuzzy logic echo classifier will be substituted for the A_{MET} of the additional fuzzy logic echo classifier) is shown in Fig. 11a; the decrease of A_{MET} before the post-processing in ML region is effectively suppressed. The final classification result based on A_{MET} after post-processing (Fig. 11c) shows good performance in ML region.

4 Evaluation

   In order to objectively evaluate the performance of the MetSignal_noise algorithm and its improvement compared with the

215   MetSignal algorithm, a test set independent of the training set is selected and listed in Table 4.

   The classification accuracy of the MetSignal and MetSignal_noise algorithms based on data in the test set is shown in Table 5. In order to facilitate the analysis of the dependence between classification performance and SNR, the statistics of classification accuracy is stratified by three SNR intervals (larger than 15 dB, 5–15 dB, and larger than 5 dB). By comparing the classification performance of the two algorithms in MET, it can be found that the classification accuracy of

220   MetSignal_noise algorithm is significantly higher than that of the MetSignal algorithm, especially in the SNR interval greater than 5 dB and less than 15 dB. This can verify that the MetSignal_noise algorithm can improve the classification

performance of the MetSignal algorithm at low SNR by stratifying polarimetric features based on SNR intervals and masking low SNR polarimetric variables in texture calculation. The better performance of the MetSignal_noise algorithm in the SNR interval greater than 15 dB is mainly owed to the fact that membership functions of polarimetric features are more
225   targeted after SNR stratification. Compared with the differences in MET between the two algorithms, the difference in NMET is much smaller. The classification performance of the MetSignal algorithm in NMET is slightly better than that of the MetSignal_noise algorithm in the SNR interval greater than 5 dB and less than 15 dB, which should be attributed to the misclassification of CA into MET in the potential ML regions after post-processing because of non-polarimetric features (i.e., Z, V, and SD(Z)) cannot effectively distinguish CA from MET (Lakshmanan et al. 2007; Tang et al. 2014). The main reason
230   for the lower MetSignal algorithm classification accuracy in the SNR interval greater than 15 dB is that the Z of AP is sometimes more than 11 dBZ at 3 km and will be classified as MET in the post-processing of the MetSignal algorithm.

4 Conclusions

An improved fuzzy logic method, MetSignal_noise, is proposed in this paper to distinguish between MET and NMET using polarimetric radar data from NUIST-CDP. The most significant improvement over the raw version (MetSignal) is its better
235   classification performance in weak signal regions by stratifying polarimetric features based on SNR intervals and masking low SNR polarimetric variables in texture calculation. In addition, the thresholds of Z and W are set to limit the use scope of V, so as to improve the classification performance of V and prevent its contribution to the misclassification of CA. An averaging method along the radial is also used to decrease the abnormal high value of CC from GC and AP. The post-processing rule used to prevent misclassification in ML regions in the MetSignal algorithm sometimes reclassifies AP at far
240   range into MET, therefore, it has been removed in the MetSignal_noise algorithm, and its substitute, that is an additional fuzzy logic echo classifier without the polarimetric features input, is implemented in post-processing of MetSignal_noise.
An independent test set is selected to evaluate algorithm performance; the results show that the MetSignal_noise algorithm is better than the MetSignal algorithm on the whole, especially in low SNR regions. However, the MetSignal_noise algorithm is slightly worse than the MetSignal algorithm in SNR intervals greater than 5 dB and less than 15 dB. This is because some
245   CA are reclassified as MET after post-processing because non-polarimetric features cannot effectively distinguish CA from MET. Although increasing the height threshold of the potential ML region can improve this defect as CA does not usually appear at high altitudes (Wilson et al. 1994), this will cause some low ML regions to miss the post-processing. In addition, the altitude of ML also depends on the season and geographical location (Zhang and Qi 2010). Therefore, real-time ML identification algorithms (Giangrande et al. 2008; Zhang et al. 2008) or atmospheric environmental data (Tang et al. 2014)
250   have been considered as additions to the MetSignal_noise algorithm in the following study to select a better height threshold. In addition, it is planned to identify and eliminate the second-trip echo in future work to further improve data quality.

References

Bringi, V. N. and Chandrasekar, V.: Polarimetric Doppler Weather Radar, Cambridge University Press, 2001.

255 Cho, Y. H., Lee, G., Kim, K. E., and Zawadzki, I.: Identification and Removal of Ground Echoes and Anomalous Propagation Using the Characteristics of Radar Echoes, Journal of Atmospheric & Oceanic Technology, 23, 1206-1222, 2006.

Crum, T. D. and Alberty, R. L.: The WSR-88D and the WSR-88D Operational Support Facility, Bulletin of the American Meteorological Society, 74, 1669-1688, 1993.

Doviak, R. J. and Zrnic´, D. S.: Doppler radar and weather observations, Academic Press, Mineola, N.Y., 2nd ed., dover ed.
260 edn., 2006.

Fang, M., Doviak, R. J., and Melnikov, V.: Spectrum Width Measured by WSR-88D: Error Sources and Statistics of Various Weather Phenomena, Journal of Atmospheric & Oceanic Technology, 21, 888-904, 2004.

Giangrande, S. E., and Ryzhkov, A. V.: Estimation of Rainfall Based on the Results of Polarimetric Echo Classification, Journal of Applied Meteorology & Climatology, 47, 2445-2462, 2008.

265 Giangrande, S. E., Krause, J., and Ryzhkov, A. V: Automatic detection of the melting layer with a polarimetric prototype of the WSR-88D radar, Preprints, 47, 1354-1364, 2008.

Gourley, J. J., Tabary, P., and Chatelet, J. P. D.: Data Quality of the Meteo-France C-Band Polarimetric Radar, Journal of Atmospheric & Oceanic Technology, 23, 1340, 2006.

Gourley, J. J., Tabary, P., and Parent du Chatelet, J.: A Fuzzy Logic Algorithm for the Separation of Precipitating from Non-
270 precipitating Echoes Using Polarimetric Radar Observations, Journal of Atmospheric and Oceanic Technology, 24, 1439–1451, 2007.

Islam, T., Rico-Ramirez, M. A., Han, D., and Srivastava, P. K.: Artificial intelligence techniques for clutter identification with polarimetric radar signatures, Atmospheric Research, 109-110, 95-113, 2012.

Jung, Y., Zhang, G., and Xue, M.: Assimilation of simulated polarimetric radar data for a convective storm using the
275 ensemble Kalman filter. Part I: Observation Operators for Reflectivity and Polarimetric Variables, Monthly Weather Review, 136, 2228-2245, 2008.

Jung, Y., Zhang, G., and Xue, M.: Assimilation of simulated polarimetric radar data for a convective storm using the ensemble Kalman filter. Part II: Impact of polarimetric data on storm analysis, Monthly Weather Review, 136, 2246-2260, 2008.

280 Krause, J. M.: A Simple Algorithm to Discriminate between Meteorological and Nonmeteorological Radar Echoes, Journal of Atmospheric & Oceanic Technology, 33, 1875-1885, 2016.

Kumjian, M. R.: Principles and Applications of Dual-Polarization Weather Radar. Part I: Description of the Polarimetric Radar Variables, 1, 226-242, 2013.

Kumjian, M. R.: Principles and Applications of Dual-Polarization Weather Radar. Part II: Warm-and Cold-Season
285   Applications, Journal of Operational Meteorology, 1, 243-264, 2013.

Kumjian, M. R.: Principles and Applications of Dual-Polarization Weather Radar. Part III: Artifacts, Journal of Operational
Meteorology, 1, 265-274, 2013.

Lakshmanan, V., Fritz, A., Smith, T., Hondl, K., and Stumpf, G.: An Automated Technique to Quality Control Radar
Reflectivity Data, Journal of Applied Meteorology & Climatology, 46, 288-305, 2007.

290   Lakshmanan, V., Karstens, C., Krause, J., and Tang, L.: Quality Control of Weather Radar Data Using Polarimetric
Variables, Journal of Atmospheric & Oceanic Technology, 31, 1234-1249, 2014.

Lakshmanan, V., Karstens, C., Krause, J., Elmore, K., Ryzhkov, A., and Berkseth, S.: Which Polarimetric Variables Are
Important for Weather/No-Weather Discrimination?, Journal of Atmospheric & Oceanic Technology, 32, 1209-1223, 2015.

Lin, P. F., Chang, P. L., Jou, J. D., Wilson, J. W., and Roberts, R. D.: Objective Prediction of Warm Season Afternoon
295   Thunderstorms in Northern Taiwan Using a Fuzzy Logic Approach, Weather & Forecasting, 27, 1178-1197, 2012.

Liu, H., and Chandrasekar, V.: Classification of hydrometeors based on polarimetric radar measurements: Development of
fuzzy logic and neuro-fuzzy systems, and in situ verification, Journal of Atmospheric and Oceanic Technology, 17, 140-164,
2000.

Park, H., Ryzhkov, A. V., Zrnic, D. S., and Kim, K. E.: The Hydrometeor Classification Algorithm for the Polarimetric
300   WSR-88D: Description and Application to an MCS, Weather & Forecasting, 24, 730-748, 2009.

Rico-Ramirez, M. A., and Cluckie, I. D.: Classification of Ground Clutter and Anomalous Propagation Using Dual-
Polarization Weather Radar, IEEE Transactions on Geoscience & Remote Sensing, 46, 1892-1904, 2008.

Ryzhkov, A. V., Giangrande, S. E., Melnikov, V. M., and Schuur, T. J.: Calibration Issues of Dual-Polarization Radar
Measurements, Journal of Atmospheric & Oceanic Technology, 22, 1138-1155, 2005.

305   Schuur, T., Ryzhkov, A., Heinselman, P., Zrnic, D., Burgess, D., and Scharfenberg, K.: Observations and classification of
echoes with the polarimetric WSR-88D radar, Report of the National Severe Storms Laboratory, Norman, OK, 73069, 46,
2003.

Stumpf, G. J., Witt, A., Mitchell, D. W., Spencer, P. L., and Burgess, D. W.: The National Severe Storms Laboratory
Mesocyclone Detection Algorithm for the WSR-88D, Weather & Forecasting, 13, 304-326, 1998.

310   Tang, L., Zhang, J., Langston, C., Krause, J., Howard, K., and Lakshmanan, V.: A Physically Based Precipitation-
Nonprecipitation Radar Echo Classifier Using Polarimetric and Environmental Data in a Real-Time National System,
Weather & Forecasting, 29, 1106-1119, 2014.

Wang, Y. T., and Chandrasekar, V.: Algorithm for estimation of the specific differential phase, Journal of Atmospheric &
Oceanic Technology, 26, 2565-2578, 2009.

315   Wilson, J. W., Weckwerth, T. M., Vivekanandan, J., Wakimoto, R. M., and Russell, R. W.: Boundary Layer Clear-Air Radar
Echoes: Origin of Echoes and Accuracy of Derived Winds, Journal of Atmospheric & Oceanic Technology, 11, 1184-1206,
1994.

Zhang, J., and Qi, Y. C.: A real-time algorithm for the correction of brightband effects in radar-derived QPE, Journal of Hydrometeorology, 11, 1157-1171, 2010.

320   Zhang, J., Howard, K., Langston, C., Vasiloff, S., Kaney, B., Arthur, A., Cooten, S. V., Kelleher, K., Kitzmiller, D., and Feng, D.: National Mosaic and Multi-Sensor QPE (NMQ) System: Description, Results, and Future Plans, Bulletin of the American Meteorological Society, 92, 1321-1338, 2011.

Zhang, J., Langston, C., and Howard, K.: Brightband Identification Based on Vertical Profiles of Reflectivity from the WSR-88D, Journal of Atmospheric & Oceanic Technology, 25, 1859-1872, 2008.

325   Zrnic, D. S., Melnikov, V. M., and Ryzhkov, A. V.: Correlation Coefficients between Horizontally and Vertically Polarized Returns from Ground Clutter, Journal of Atmospheric & Oceanic Technology, 23, 381-394, 2006.

Zrnic, D. S., Ryzhkov, A., Straka, J., Liu, Y., and Vivekanandan, J.: Testing a Procedure for Automatic Classification of Hydrometeor Types, Journal of Atmospheric & Oceanic Technology, 18, 892-913, 2001.

330

TABLE 1: Main parameters of NUIST-CDP.

Parameters	NUIST-CDP
Transmitter	Klystron (5,600 MHz)
Pulse width	0.5 us
PRF	1,000 Hz
Peak power	250 kW
Receiver	Simultaneous Horizontal/Vertical
Noise figure	3 dB
Dynamic range	90 dB
Sensitivity	-109 dBm
Antenna feeder	Paraboloid
Antenna gain	48.5 dB
Reflector diameter	8.5 m
Beam width	0.54°

335   **TABLE 2: The weight setting for each feature in the MetSignal algorithm.**

Feature	Weight
Z	1
V	1
CC	1
SD(ZDR)	2
SD(CC)	1

TABLE 3: List of events used for training membership functions (UTC).

Date	Description
00:00–01:00 1 May 2017	AP
01:00–02:00 2 May 2017	stratiform precipitation
04:00–05:00 3 May 2017	CA
14:00–15:00 3 May 2017	convective precipitation
18:00–19:00 4 May 2017	GC
20:00–21:00 5 May 2017	stratiform precipitation
00:00–01:00 6 May 2017	GC
08:00–09:00 6 May 2017	stratiform precipitation
06:00–07:00 7 May 2017	CA
18:00–19:00 7 May 2017	convective precipitation
22:00–23:00 8 May 2017	GC
01:00–02:00 11 May 2017	AP
09:00–10:00 11 May 2017	convective precipitation

17:00–18:00 11 May 2017	stratiform precipitation
13:00–14:00 12 May 2017	CA
22:00–23:00 13 May 2017	AP
06:00–07:00 14 May 2017	convective precipitation
17:00–18:00 14 May 2017	stratiform precipitation
01:00–02:00 15 May 2017	CA
22:00–23:00 16 May 2017	AP
14:00–15:00 18 May 2017	CA
09:00–10:00 19 May 2017	stratiform precipitation
08:00–09:00 20 May 2017	convective precipitation

340

TABLE 4: List of events used for evaluating algorithm performance (UTC).

Date	Description
04:00–05:00 21 May 2017	CA
09:00–10:00 22 May 2017	convective precipitation
05:00–06:00 23 May 2017	stratiform precipitation
22:00–23:00 23 May 2017	GC
22:00–23:00 24 May 2017	AP
22:00–23:00 26 May 2017	AP
12:00–13:00 28 May 2017	CA
05:00–06:00 30 May 2017	stratiform precipitation
10:00–11:00 30 May 2017	convective precipitation
22:00–23:00 31 May 2017	stratiform precipitation

345

TABLE 5: The classification accuracy of MetSignal and MetSignal_noise algorithms based on data in test set.

	MetSignal		MetSignal_noise	
	MET	NMET	MET	NMET
5 < SNR < 15 [dB]	67.1 %	96.3 %	98.3 %	94.9 %
SNR > 15 [dB]	97.5 %	96.7 %	99.6 %	98.4 %
SNR > 5 [dB]	78.4 %	96.5 %	98.8 %	97.1 %

350
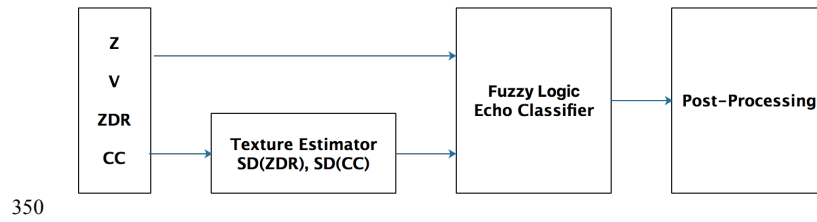
Figure 1: Block diagram of the MetSignal algorithm.
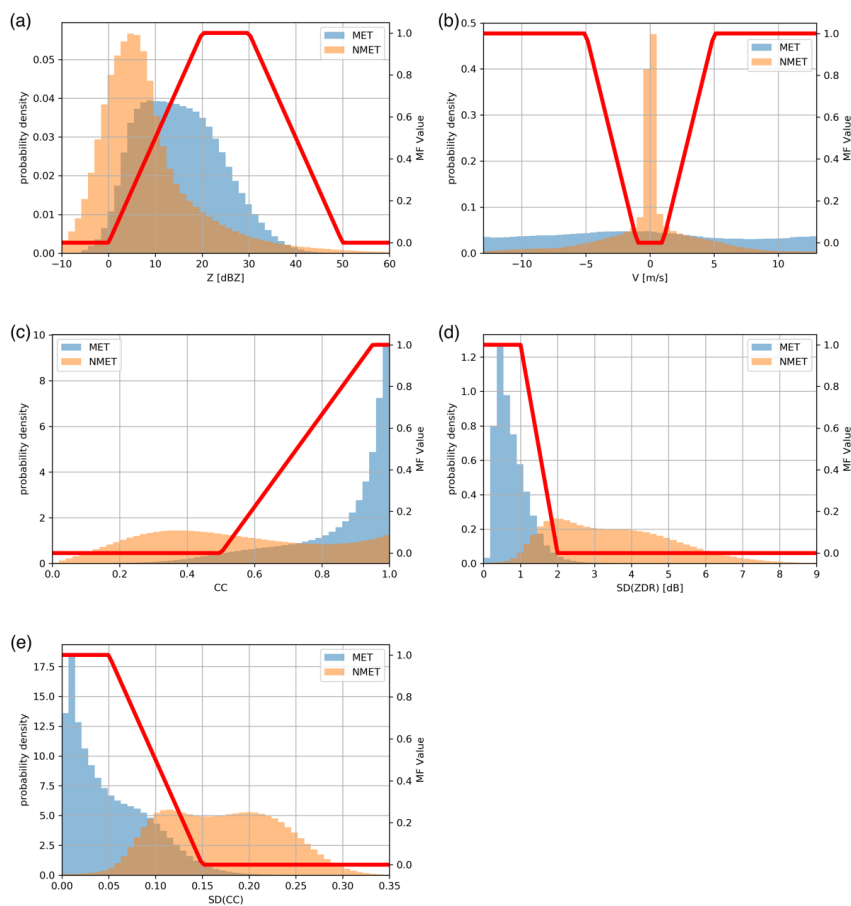
355

Figure 2: The normalized frequency distributions and membership functions of features. (a) Z, (b) V, (c) CC, (d) SD(ZDR), and (e) SD(CC).
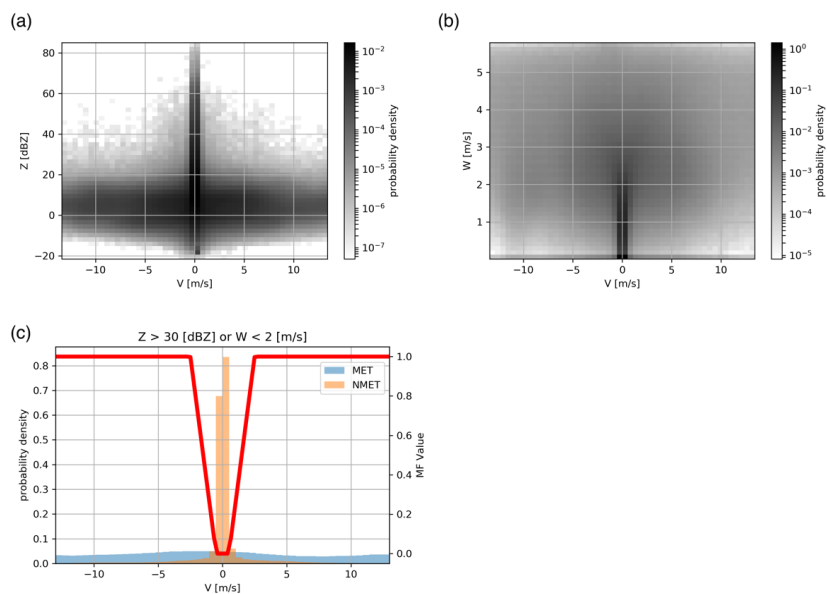
360

Figure 3: (a) The 2D histogram of V vs Z of NMET. (b) The 2D histogram of V vs W of NMET. (c) The normalized frequency distribution and membership function of V after setting thresholds of Z and W.
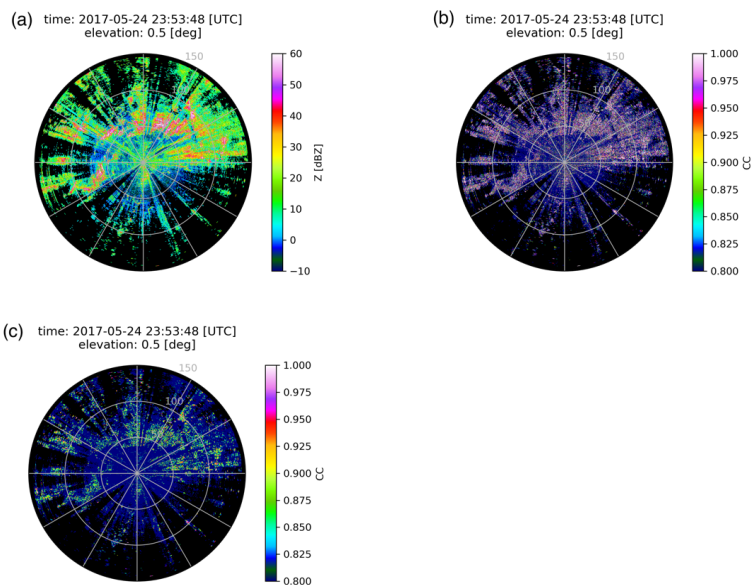
365

Figure 4: (a) Z, (b) CC, and (c) CC after averaging along the radial using a 1.5-km window. All from the NUIST-CDP radar at 23:53 UTC 24 May 2017 from an elevation of 0.5°.
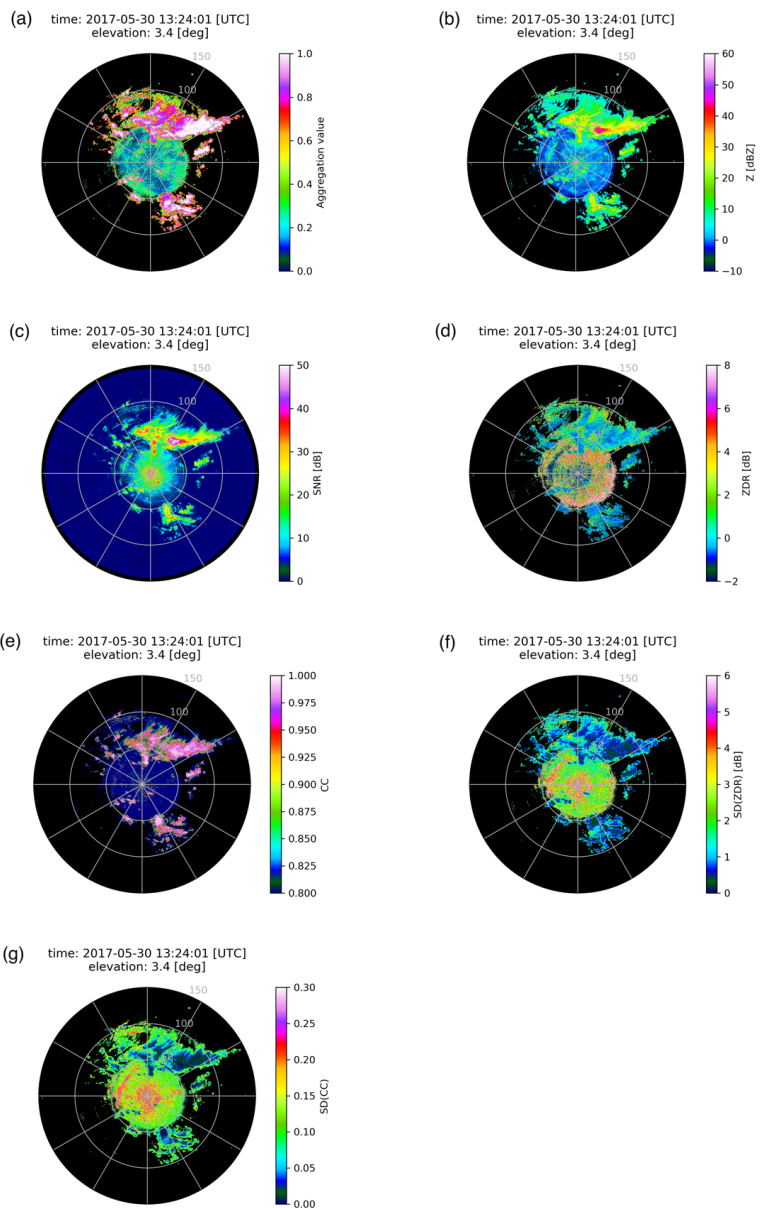
370

Figure 5: (a) AMET (MetSignal), (b) Z, (c) SNR, (d) ZDR, (e) CC, (f) SD(ZDR), and (g) SD(CC). All from the NUIST-CDP radar at 13:24 UTC 30 May 2017 from an elevation of 3.4°.

375
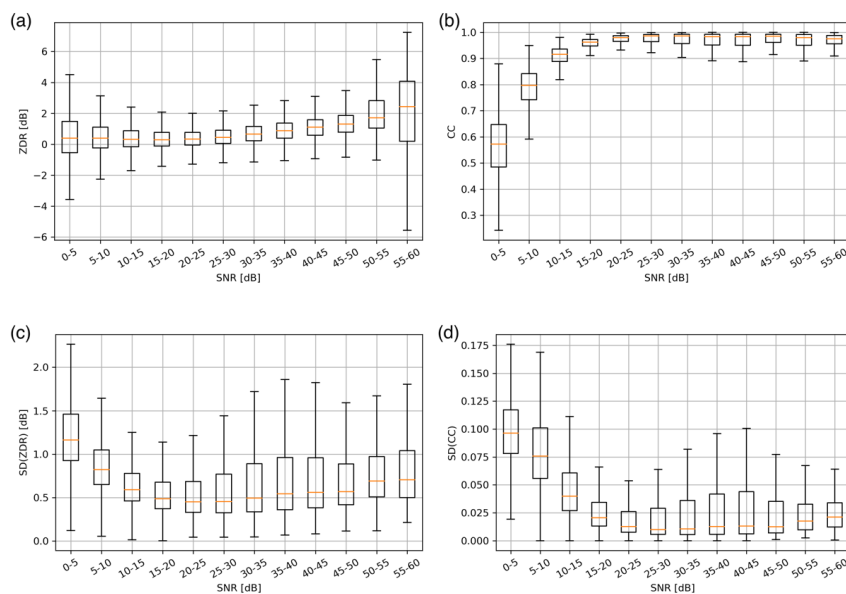
Figure 6: The boxplot of SNR vs polarimetric features of MET. (a) ZDR, (b) CC, (c) SD(ZDR), and (d) SD(CC).

380
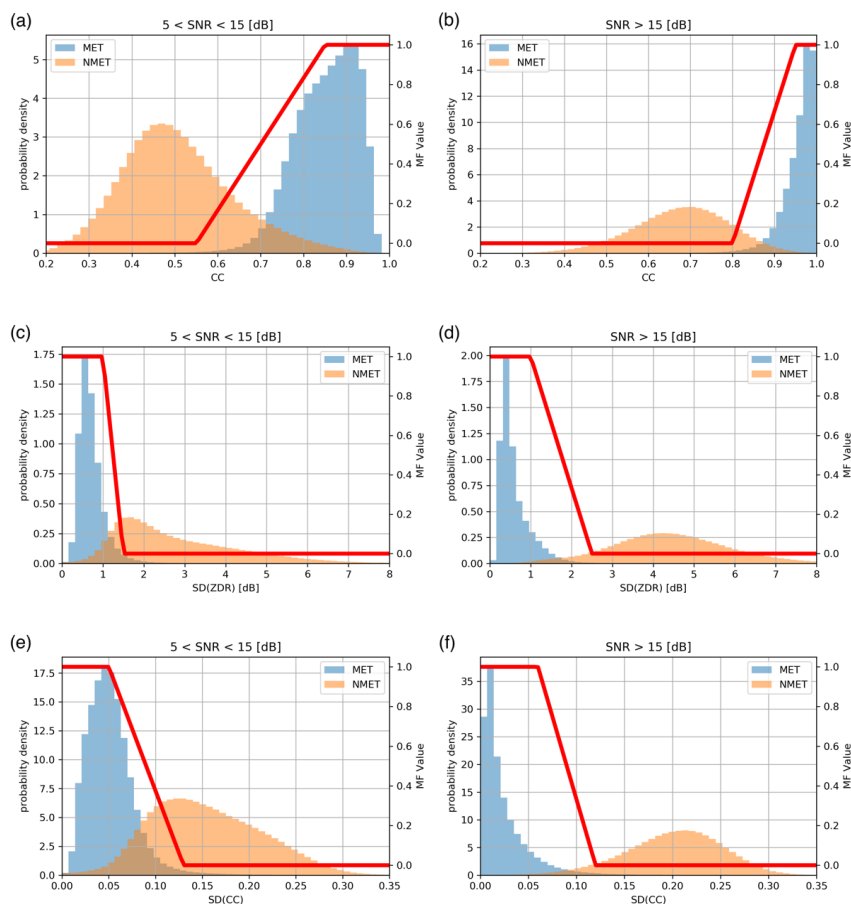
Figure 7: The normalized frequency distributions and membership functions of polarimetric features stratified by SNR. (a) CC (5 < SNR < 15 dB), (b) CC (SNR >15 dB), (c) SD(ZDR) (5 < SNR < 15 dB), (d) SD(ZDR) (SNR >15 dB), (e) SD(CC) (5 < SNR < 15 dB), and (f) SD(CC) (SNR >15 dB).

385

390
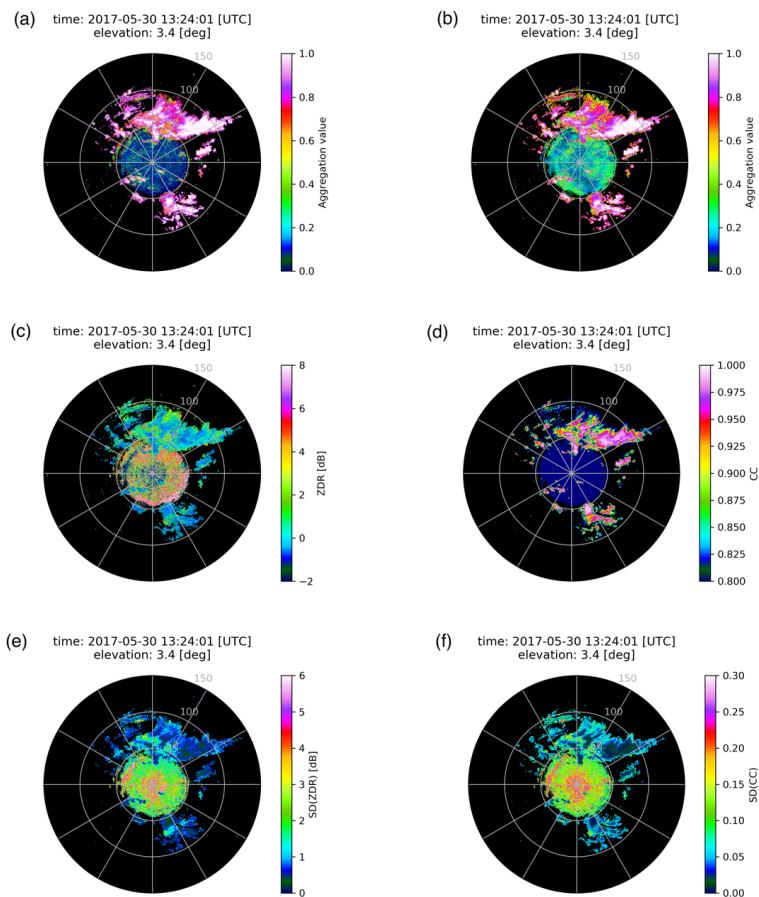
Figure 8: (a) A_{MET} (MetSignal_noise), (b) AMET (MetSignal) after masking SNR less than 5 dB, (c) ZDR after masking SNR less than 5 dB, (d) CC after averaging along the radial using a 1.5-km window and masking SNR less than 5 dB, (e) SD(ZDR) after 395 **masking SNR less than 5 dB, and (f) SD(CC) after masking SNR less than 5 dB. All from the NUIST-CDP radar at 1324 UTC 30 May 2017 from an elevation of 3.4°.**

400
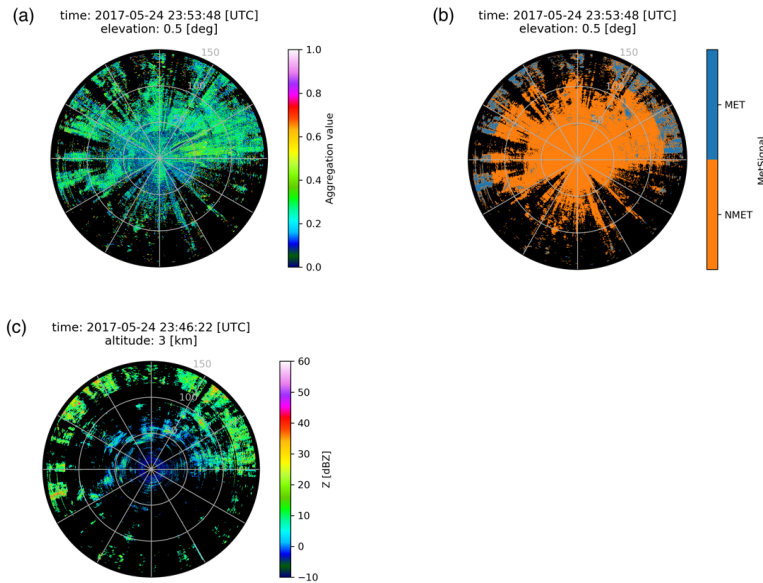
Figure 9: (a) AMET (MetSignal), (b) MetSignal, and (c) The CAPPI of Z at the altitude of 3 km. (a) and (b) from the NUIST-CDP radar at 23:53 UTC 24 May 2017 from an elevation of 0.5° while (c) at 23:46 UTC 24 May 2017 (the previous volume scan of (a) and (b)).

405
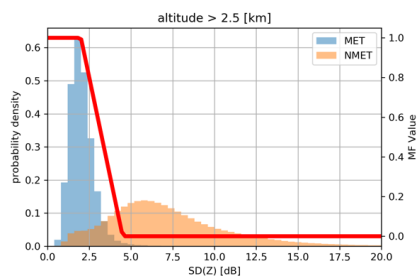
410

Figure 10: The normalized frequency distribution and membership function of SD(Z) in the regions over 2.5 km in height.

415
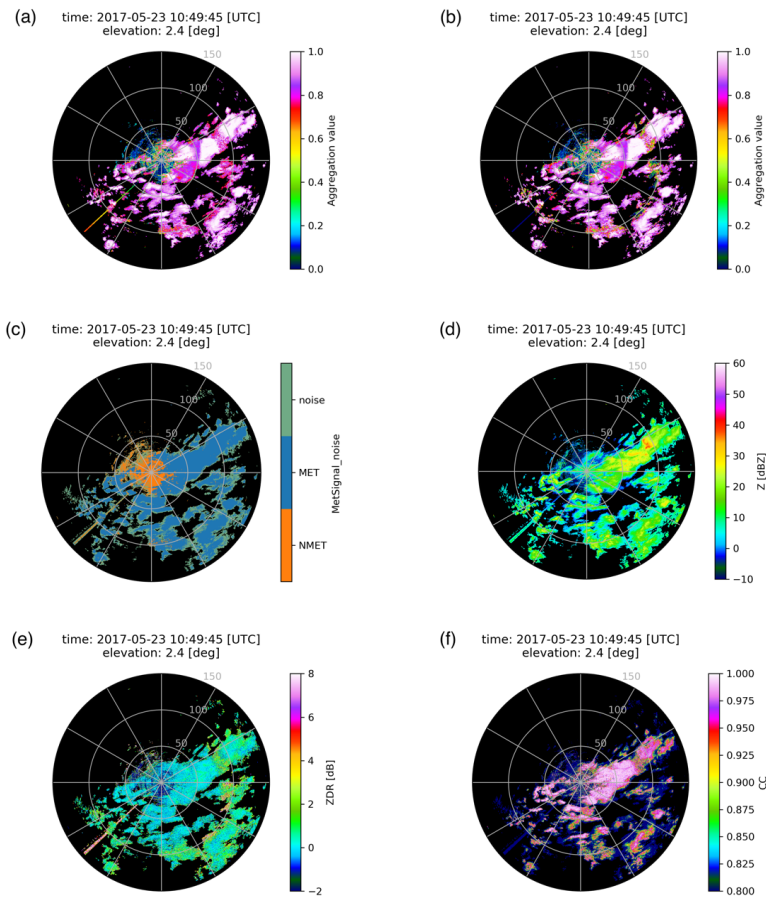
Figure 11: (a) AMET (MetSignal_noise) after post-processing, (b) AMET (MetSignal_noise) before post-processing, (c) MetSignal_noise, (d) Z, (e) ZDR, and (f) CC. All from the NUIST-CDP radar at 10:49 UTC 23 May 2017 from an elevation of 2.4°.